Magnetospheric considerations for solar system ice state

Journal Item

Icarus 302 (2018) 560–564

Contents lists available at ScienceDirect

Icarus

journal homepage: www.elsevier.com/locate/icarus

Magnetospheric considerations for solar system ice state

C. Paranicas[a,*], C.A. Hibbitts[a], P. Kollmann[a], N. Ligier[b], A.R. Hendrix[c], T.A. Nordheim[d], E. Roussos[e], N. Krupp[e], D. Blaney[d], T.A. Cassidy[f], G. Clark[a]

[a] APL, 11100 Johns Hopkins Rd., Laurel, MD 20723, USA
[b] Open University, UK
[c] Planetary Science Institute, Tucson, AZ, USA
[d] Jet Propulsion Laboratory, Pasadena, CA, USA
[e] Max-Planck-Institut fuer Sonnensystemforschung MPS, Goettingen, Germany
[f] Laboratory for Atmospheric and Space Physics, University of Colorado, USA

ARTICLE INFO

Article history:
Received 26 May 2017
Revised 3 November 2017
Accepted 7 December 2017
Available online 9 December 2017

ABSTRACT

The current lattice configuration of the water ice on the surfaces of the inner satellites of Jupiter and Saturn is likely shaped by many factors. But laboratory experiments have found that energetic proton irradiation can cause a transition in the structure of pure water ice from crystalline to amorphous. It is not known to what extent this process is competitive with other processes in solar system contexts. For example, surface regions that are rich in water ice may be too warm for this effect to be important, even if the energetic proton bombardment rate is very high. In this paper, we make predictions, based on particle flux levels and other considerations, about where in the magnetospheres of Jupiter and Saturn the ~MeV proton irradiation mechanism should be most relevant. Our results support the conclusions of Hansen and McCord (2004), who related relative level of radiation on the three outer Galilean satellites to the amorphous ice content within the top 1 mm of surface. We argue here that if magnetospheric effects are considered more carefully, the correlation is even more compelling. Crystalline ice is by far the dominant ice state detected on the inner Saturnian satellites and, as we show here, the flux of bombarding energetic protons onto these bodies is much smaller than at the inner Jovian satellites. Therefore, the ice on the Saturnian satellites also corroborates the correlation.

1. Introduction

The magnetospheres of Jupiter and Saturn contain the most intense fluxes of energetic charged particles close to the planet and near the magnetic equator. Icy satellites are present deep in these magnetospheres and their surfaces are continuously weathered by charged particles. These interactions can modify the ice in a number of ways including by sputtering it (e.g., Cassidy et al., 2013), destroying its crystallinity (e.g., Moore and Hudson, 1992), altering its thermal properties through the deposition of energy (e.g., Howett et al., 2011), and creating new molecules, such as peroxide (e.g., Carlson et al., 1999; Moore and Hudson, 2000; Hand and Carlson, 2011). In this paper, we will focus on predicting which satellites in the inner to middle magnetospheres of Jupiter and Saturn will likely be most affected by energetic protons that can modify the ice lattice.

Previously, several researchers have documented surface characteristics resulting from bombardment by magnetospheric particles. Hansen and McCord (2004) carried out analyses of reflectance spectra of the surfaces of the three outer Galilean satellites using data from the Galileo Near-Infrared Mapping Spectrometer (NIMS). They concluded that among them, the one that is closest to the Jovian radiation belts (Europa, r ~ 9.4 R_J, where $R_J = 71{,}492$ km) and subject to the most radiation, also has the most amorphous ice. This was based on the nature of the 3.1 μm Fresnel reflection peak in ice that probes the upper microns of the grains in the regolith. The percentage of amorphous ice in the outer portion of the grains decreases for Ganymede (r ~ 14.9 R_J). For Callisto (r ~ 26.3 R_J), only crystalline ice is detected. Hansen and McCord (2004) further found through the analysis of the 1.65 μm water ice feature, that ice grains are crystalline in their interiors such that amorphous ice, when present, is limited to the very top surface. At a depth of 1 mm and deeper, all water ice on these three satellites is crys-

* Corresponding author.
E-mail address: chris.paranicas@jhuapl.edu (C. Paranicas).

https://doi.org/10.1016/j.icarus.2017.12.013

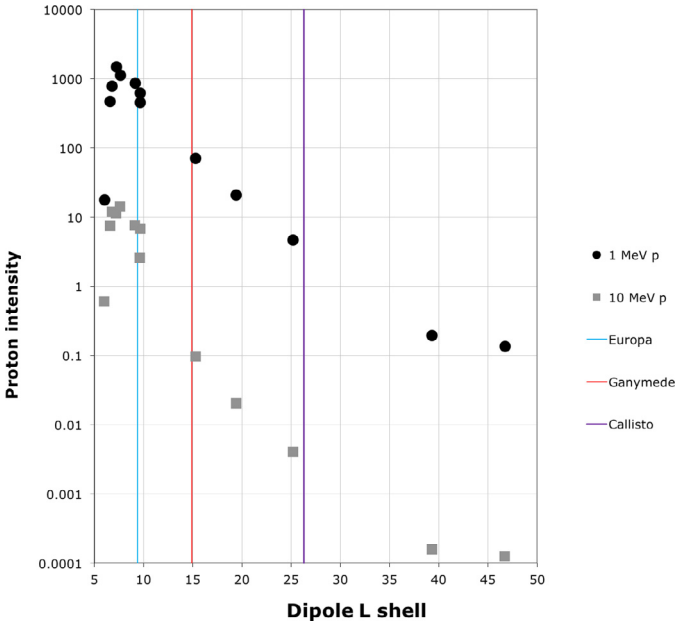

Fig. 1. Proton intensities versus dipole L shell for 1 MeV and 10 MeV protons. These points are derived from fit functions to the Galileo EPD data created by Mauk et al. (2004). Units are protons per cm^2-s-sr-keV.

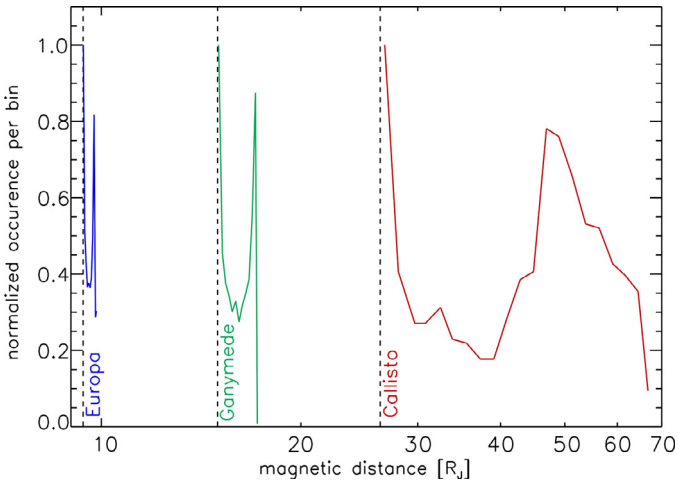

Fig. 2. Histogram of magnetic distances covered by Europa, Ganymede, and Callisto during their orbits around Jupiter. Each moon location is traced in the Khurana magnetic field model to the minimum B point. The radial distances of these magnetic equator points are shown on the x-axis. The occurrence of the distances is sampled in logarithmic bins, normalized to the maximum, and shown on the y-axis.

talline. This interpretation of only crystalline water ice (at depth) is also supported by Earth based telescopic observations (Ligier et al., 2016).

While Hansen and McCord (2004) pointed out that energetic ion bombardment is only one mechanism for transforming crystalline ice to amorphous ice, the increasing crystallinity of surface ice correlating with the satellites' Jovian distance makes this mechanism a very likely explanation. Furthermore, the crystalline-to-amorphous transition has been demonstrated in laboratory experiments in which water ice is bombarded with protons (Moore and Hudson, 1992; Mastrapa and Brown, 2006; Fama et al., 2010). This is a useful piece of the puzzle even though the laboratory data are not all completely consistent with each other. Finally, the penetration depth of energetic protons and heavy ions in ice is very shallow, as is the amorphous ice feature. A depth of 20 μm, for instance, is sensed by the 3 μm feature.

2. Charged particle bombardment of the three outer Galilean satellites

The fall-off of energetic ion flux from the orbit of Europa to that of Callisto correlates with the percentage of amorphous ice on the surface, as measured by the 3.05 μm Fresnel reflection peak in the ice. In this section, we will take a more comprehensive look at the relevant satellite environments.

In Fig. 1, we show the behavior of the intensity of 1 and 10 MeV protons at dipole L shells between 5 and 50 R_J. In a dipole model of the magnetic field, L (expressed in planetary radii) is the distance at which magnetic field lines associated with that L shell cross the magnetic equator. This plot uses the energy spectra determined by Mauk et al. (2004), who based their fits on time-of-flight and other measurements from the Galileo Energetic Particles Detector (EPD) instrument at a limited number of Jovian distances. The data show the peak intensity is located close to the orbit of Europa, falling both inward toward Jupiter and outward toward Callisto. While there is a level of variation near Europa's orbital distance, the plot shows the intensities at Callisto are at least an order of magnitude lower.

A complication of displaying proton flux as a function of dipole L shell is the planetary ring current. This current flows in the azimuthal direction and effectively stretches the magnetic field lines out of their dipolar configuration. Connerney et al. (1981) showed, using a model of the magnetic field near the current sheet, that the equatorial crossing point of the field lines can be significantly different from a dipole at equatorial distances greater 15 R_J (see their Fig. 10). Therefore Fig. 1 provides a reasonable approximation to the intensities out to about Ganymede's orbit only.

Since we are interested in comparing the charged particle weathering of Europa and Callisto, we have improved upon the dipole picture in the following way. We used representative points along the moon orbits to determine the corresponding radial distance to the point of the minimum magnetic field intensity on the field line occupied by the satellite. Because the dipolar L value is the radial distance to the minimum B point on the field line, the minimum B point in a non-dipolar magnetic field is a way to associate each magnetic field line with a radial distance. Magnetic field lines with a larger minimum B distance would, for example, be less likely to sustain high fluxes of trapped charged particles. We computed minimum B points in the Khurana magnetic field model (Khurana, 1997), which includes non-dipolar terms of Jupiter's intrinsic field and accounts for time-varying ring and other current systems. We sampled positions along the orbits of Europa, Ganymede, and Callisto, and traced these points along the model magnetic field line to its minimum B distance. By doing so, we found the following range of distances at which the minimum B point is located: Europa (9.3 to 10.0 R_J), Ganymede (15.0 to 17.4 R_J) and Callisto (26 to 69 R_J). A histogram of the time spent at each distance is shown in Fig. 2.

In a dipolar magnetic field, the nearly 10° tilt between the magnetic equator and the orbital plane of the satellites means the moons occupy a range of dipole L shells during their orbits. As noted, for very stretched magnetic field lines this range can dramatically increase. At the same time, trapped flux tends to become less intense with increasing distance from Jupiter. In addition, some of the flux on stretched field lines will be confined to the region near the magnetic equator and never reach the satellite. Therefore, in addition to the fall-off of flux that would be approximated using the dipole L in Fig. 1, these factors suggest that the weathering rate of Callisto by energetic charged particles is likely orders of magnitude smaller than the rate at Europa.

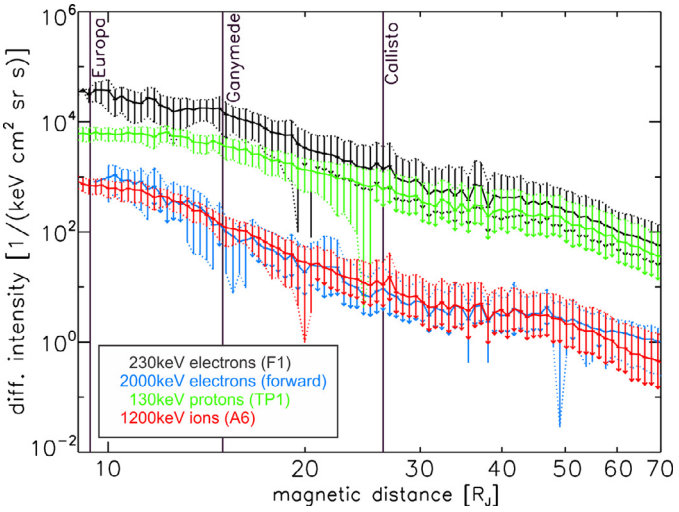

Fig. 3. Mission-averaged intensities of 230 keV electrons (black), 2 MeV electrons (blue), 130 keV protons (green), and 1.2 MeV total ions (red) versus magnetic distance (see Fig. 2). Data were taken by the EPD/LEMMS and CMS instruments and have been corrected for background contamination and instrument saturation (so-called *r-vs-r* effects). The 2 MeV electron intensities are based on a forward model constrained by integral channels. Averages are linear with a median filter; the error bars show the 1-sigma standard deviation and illustrate the variability of the magnetosphere. Error bars with a downward pointing arrow indicate a standard deviation extending below the range of intensity shown. (For interpretation of the references to colour in this figure legend, the reader is referred to the web version of this article.)

In Fig. 3, we organize the intensities that were measured at different locations in the same way we organized the moon locations. This figure shows mission-averaged intensities from Galileo EPD of 130 keV protons, 1.2 MeV ions, and 230 keV and 2 MeV electrons. The data are plotted by tracing from Galileo's position at the time of the measurement to the minimum B point on the field line in the Khurana model, exactly as we have done for the satellite orbits. By doing this tracing, it is easier to understand the range of measured fluxes that a satellite is exposed to during its orbit. We include energetic electrons for comparison.

Without the stretching of the magnetic field lines, the intensity fall-off between Europa and Callisto is an order of magnitude or so in the quantities shown in Fig. 3; Hansen and McCord (2004) estimated the value as 32. However, if it is recognized that Callisto moves on and off of magnetic field lines with minimum B distances that can be as large as 70 R_J, two things become apparent. First, the weathering of Callisto by energetic particles varies by orders of magnitude during each rotation of the planet in Callisto's reference frame. Second, because the same variation does not occur on Europa, the difference in weathering between those two satellites is more accurately several orders of magnitude. We suggest here that the stretching caused by the circumplanetary currents is a dominant factor in reducing the charged particle weathering rates onto Callisto.

Finally, at Ganymede, the situation is complicated by the moon's internal magnetic field. Ganymede is close to Europa and also has a very narrow excursion in minimum B (see Fig. 2). All else being equal, we might expect Ganymede's ice to be weathered in a similar way to Europa's. But the moon's own magnetic field alters the trajectories of magnetospheric charged particles as they approach it. Allioux et al. (2013) found a decrease in the access of hundreds of keV ions to Ganymede's surface that varied with location. Galileo data supported this claim, finding magnetospheric intensities dropped near the moon. Khurana et al. (2007) also pointed out differences in the surface reflectance properties that they related to weathering differences and particle access along open versus closed Ganymede field lines. Hansen and McCord (2004) found more amorphous ice in a portion of the polar region and in the equatorial trailing region. It is likely that a more complete simulation is needed to model the access to Ganymede's surface by the relevant ions.

3. Charged particle bombardment of the inner Saturnian satellites

On the Saturnian satellites, most of the surface ice observed in the 1 to 5 μm spectral range is in the crystalline state, implying there is very little amorphous ice even on the very outside of grain surfaces (e.g., Clark et al., 2012; Newman et al., 2008; Scipioni et al., 2017). At Saturn, the active moon Enceladus is a source of the particles that make up the E ring, which coexists with the orbits of the inner satellites. Buratti et al. (1990) suggested that the inner moons of Saturn would likely be coated with the E ring ice grains. Optical studies on the brightness of the satellites nearest to Enceladus: Mimas, Tethys, and Dione, support this prediction (Verbiscer et al., 2007).

If the vast majority of the ice in the Saturnian system is crystalline, it suggests that the E ring grains are also crystalline. These grains have a long transit time between Enceladus and the surrounding satellite surfaces. During this period of time, they are weathered by magnetospheric ions and electrons. Smaller grains can be destroyed by sputtering (e.g., see discussion in Cassidy et al., 2013). But apparently grains that survive this irradiation do not have their ice structure altered in a meaningful way or there is a compensating process occurring. It is important to recognize that the fluxes of energetic protons are typically much lower near the inner satellites of Saturn than they are at Europa. For example, the intensity of 1 MeV protons near the inner Saturnian satellites (Paranicas et al., 2012) is several orders of magnitude below that at Ganymede, shown in Fig. 1. Fama et al. (2010) recognized that the charged particle fluxes were much different at the two planets and predicted lower levels of amorphous ice in the Saturnian system.

It is useful to note that the grain dynamics suggest that the neighboring satellites of Enceladus will not be coated in a uniform way (e.g., Hamilton and Burns, 1994). For example, the satellites inward of Enceladus (such as Janus and Mimas) are expected to receive a much higher flux of grains onto their trailing hemispheres. It is possible in principle that the top mm of surface ice on the inner Saturnian moons therefore varies in age a great deal and may have different properties.

For the mechanism we are considering here, the energetic protons have their highest intensities near Saturn. But due to the alignment of the dipole and spin axes at Saturn, it has been found that very energetic protons (which re-encounter the inner moons every few hours) have very low fluxes along the moon orbits (e.g., Kollmann et al., 2013). This is very different from the situation at Jupiter, where the intensities along the moon orbits are not that different from the surrounding regions.

In Fig. 4, we show mission-averaged intensities of 1.1 MeV ions (likely dominated by protons) obtained by the Cassini Magnetosphere Imaging Instrument (MIMI) at Saturn. Along the orbits of Janus, Mimas, and Enceladus, the proton fluxes are measured at low levels. At Dione, the flux decrease effect is not present, likely because of the faster radial transport there and the rate at which protons re-encounter that moon. These intensity minima are called *macrosignatures* because they are present along the whole moon orbit, and at Saturn extend in proton energy from the few hundreds of keV to the tens of MeV (Kollmann et al., 2013). The deep drop-outs at the moon orbits have led Roussos et al. (2008) to suggest that the inner satellites of Saturn are "isolated" in the sense

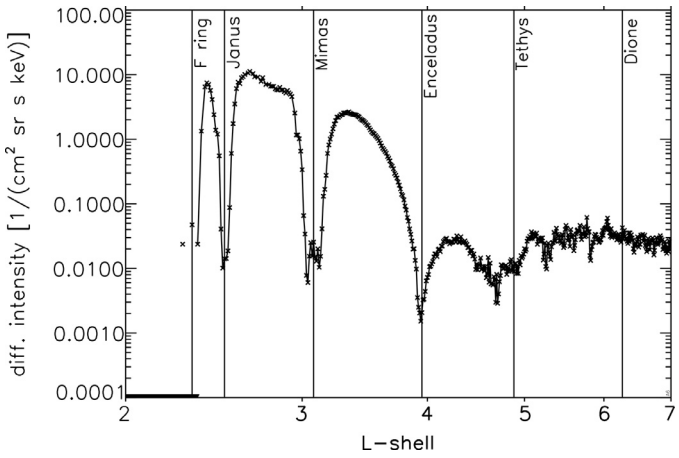

Fig. 4. Intensity of ~1.1 MeV protons versus dipole L shell at Saturn. The data are based on a linear mission-average with a median filter. Vertical lines indicate the semi-major axes of some inner moons and the F ring.

that very energetic proton populations outward of ~5 R_S cannot diffuse radially inward to these moon orbits.

Since the inner regions are isolated, it is believed that the high proton flux in Fig. 4 is caused by the cosmic ray albedo decay or CRAND process (e.g., Cooper and Simpson, 1980). Cosmic rays collide with material and create energetic neutrons, which rapidly decay into energetic protons. This source likely supplies the inner regions of the magnetosphere with energetic protons. As Fig. 4 shows, there are losses at the moon orbits as the CRAND protons diffuse radially. Since the creation of energetic protons by CRAND is a very slow process the deep macrosignatures show the diffusion is slow and therefore the weathering is at a low level. Finally, it is possible that the macrosignature sets up the conditions for more weathering onto the regions around the sub- and anti-Saturnian apex points. This concept would have to be verified by a simulation.

Based on these factors and the much lower relative proton fluxes at Saturn versus Jupiter, we expect that amorphization of surface ice by proton bombardment to be vastly less important at the Saturnian satellites.

4. Bombardment patterns

The flux at the moon's orbital distance only indicates the maximum rate that can reach a point on the surface. The bombardment pattern is needed to relate fluxes obtained in regions outside the moon's influence to the surface rates. For example, Cassidy et al. (2013) modeled the S^{++} bombardment of Europa and found a transition from mostly trailing and polar bombardment at 10 keV to nearly uniform bombardment at 10 MeV. The same kinds of patterns are expected for energetic protons.

Evidence in the remote sensing mapping observations support the idea of asymmetric particle bombardment on the satellites of the outer planets. For the Saturnian system, asymmetric electron bombardment has been correlated with near surface thermal annealing and grain welding associated with the deposition of energy (e.g., Howett et al., 2011). The "pac-man" feature on Mimas and Tethys, and to a lesser extent on Dione, appears to be the result of increased thermal inertia associated with larger grains in the surface produced from the thermal grain welding by electron "warming" of the subsurface. A global asymmetry in the albedo and abundance of non-ice material on Dione and Rhea may also be the result of asymmetric weathering. Stephan et al. (2010, 2012) hypothesize that radiation is responsible for the enhancement of non-ice material and CO_2 on the trailing hemisphere.

A good test of the hypothesis would be if the bombardment pattern of energetic protons were found to be linked to the distribution of amorphous ice on the surface. But this is complicated by several factors. The heavy energetic ions, which have their own precipitation patterns, remove ice in the very top layer (see below) and also preferentially eliminate smaller grains (e.g., Cassidy et al., 2013). In addition, the possible presence of endogenic activity, such as a plume on Europa (Roth et al., 2014; Sparks et al., 2016), may create local discrepancies in the spatial distribution of grain sizes and therefore correlations with geomorphological units (Ligier et al., 2016).

5. Discussion

In this section, we discuss other factors relevant to relating the observed amorphous ice in the top layer of some Jovian satellites to the precipitation patterns and flux levels of energetic protons. Magnetospheric processes have a much stronger effect on the spatial distribution of compositional units on the icy Galilean satellites than the Saturnian satellites because the fluxes of energetic particles in the Jovian magnetosphere tend to be significantly higher. The conspicuously ice-free nature of the uppermost layer of the trailing hemisphere of Europa (e.g., McCord et al., 1998; Hansen and McCord, 2004) is likely due to magnetospheric bombardment: either the result of sputtering (removal) of water ice resulting in the accumulation of a lag deposit of non-ice material or due to the formation and gradual accumulation of sulfuric acid hydrate (e.g., Carlson et al. 1999, 2002). A careful study of Fig. 11 of Ligier et al. (2016), with summing of the amounts in the two principal ice states, reveals the relative amounts of non-ice.

In the regions rich in water ice on Europa (i.e., mostly the leading hemisphere), there is more amorphous ice "at depth" in grains at high latitude than at low latitude. For instance, in Fig. 11a of Ligier et al. (2016), one can see this effect even though high latitude sampling is limited. The very shallow depth of the amorphous ice that is detected is consistent with protons and heavy ions being a critical agent, since they have very short ranges in materials. Other important drivers are thermal annealing, which works to return the ice to the crystalline state in higher temperature ices and a less critical factor is that the conversion to amorphous ice by irradiation has lower efficiency as temperatures near and surpass 100°K (e.g., Strazzulla et al., 1992). The temperature effect predicts that if all other factors (bombardment rate, grain size, water ice fraction, etc.) are equal, the polar regions would retain the most amorphous ice. Finally, we would like to note that the interpretation of amorphous ice by Ligier et al. (2016) is based on an assumption about the ice temperature. They have carefully considered temperature range and the small variations that can come about at other temperatures in that paper.

Ganymede's dipole magnetosphere creates an unusual situation for an airless body, resulting in the distribution of water ice unique in the Jovian and Saturnian systems. Despite its internal dipole, the trailing hemisphere of Ganymede is still subject to greater bombardment by very energetic charged particles than the leading hemisphere. This results in a lower albedo, less icy, trailing hemisphere compared to the leading hemisphere, with the water ice present being larger grained (fine-grained ice having been sputtered) and a more developed deposit of non-ice material (Hansen and McCord, 2004).

In contrast, Ganymede's polar region is more directly exposed to the trapped Jovian population, resulting in sputtering of pre-existing water ice that, due to the cold temperatures, redeposits locally. This results in more fine-grained ice. However, despite the low polar temperatures, there is no more amorphous ice at the poles of Ganymede than in the equatorial regions (Hansen and McCord, 2004). One might expect condensing water, at daytime polar

surface temperatures well below 125°K of equally bright icy terrain with direct sun exposure (e.g., Pappalardo et al., 2004), would be amorphous solid water instead of crystalline ice (Seki and Hasegawa, 1983). It is very possible that because the water condenses onto a substrate that may have remnant crystallinity, the new ice will assume a similar crystal structure, whereas laboratory experiments generally do not begin with crystalline 'seeds' as nucleation sites.

The magnetospheric effects of water ice on Callisto are minimal. For example, the leading versus trailing albedo dichotomy is minimal on Callisto (Hendrix et al., 2005). All ice on Callisto is crystalline, including the grains' surfaces. There thermal processes appear to dominate. In fact, the sublimation rate of water ice is inferred to be sufficiently rapid based on the rate of crater degradation, that a more volatile material is required to be present in the ice, such as CO_2 (Moore et al., 1996). While irradiation may not dominate the distribution of water ice on Callisto, it does appear to affect the global distribution of more volatile materials on Callisto. CO_2 on the trailing hemisphere appears to be the result of altering the non-ice material, making it trap CO_2 more efficiently, perhaps by damaging the crystal structure (e.g., Hibbitts et al., 2000). Conversely, lower S = O abundance on the trailing hemisphere suggests a minimum amount of sulfur ions present in the Jovian magnetosphere at the radial distance of Callisto.

6. Summary

A main goal of this paper was to put more quantitative constraints on the claim by Hansen and McCord (2004) that Europa's ice is subject to a much higher level of energetic proton flux than Callisto's. We agree with their conclusion but believe the much lower flux at Callisto also has to do with azimuthal currents that flow at Jupiter and stretch the field lines. This means Callisto is effectively moving through the magnetosphere and being weathered by charged particle populations that are trapped at a very wide range of Jovian distances. Spending time in the more benign radiation environment away from the magnetic equator drastically reduces the rate at which energetic protons cause crystalline ice to become amorphous.

The same processing by energetic protons of water ice would be much slower at Saturn. This is due to the facts that the Saturn radiation belts are much less intense than the Jovian ones (compare ~1 MeV protons in Figs. 3 and 4) and the main source of energetic protons on the innermost satellites is through the CRAND process and subsequent slow radial diffusion. The CRAND process likely resupplies energetic protons to the magnetosphere at a speed slower than that associated with macrosignature formation. At the same time, almost all of the water ice in the inner Saturnian system is found in the crystalline state.

Acknowledgments

The first author would like to acknowledge research grant NNX14AR26G and the second author acknowledges research grant NNX09AE72G, both grants are between NASA and the Johns Hopkins University.

References

Allioux, R., Louarn, P., Andre, N., 2013. Model of energetic populations at Ganymede, implications for an orbiter. Adv. Space Res. 51, 1204–1212.
Buratti, B.J., Mosher, J.A., Johnson, T.V., 1990. Albedo and color maps of the Saturnian satellites. Icarus 87, 339–357.
Carlson, R.W., Anderson, M.S., Johnson, R.E., Schulman, M.B., Yavrouian, A.H., 2002. Sulfuric acid production on Europa: the radiolysis of sulfur in water ice. Icarus 157, 456–463.
Carlson, R.W., et al., 1999. Hydrogen peroxide on the surface of Europa. Science 283, 2062–2064.
Cassidy, T.A., Paranicas, C.P., Shirley, J.H., Dalton III, J.B., Teolis, B.D., Johnson, R.E., Kamp, L., Hendrix, A.R., 2013. Magnetospheric ion sputtering and water ice grain size at Europa. Planet. Space Sci. 77, 64–73.
Clark, R.N., et al., 2012. The surface composition of Iapetus: mapping results from Cassini VIMS. Icarus 218, 831–860.
Connerney, J.E.P., Acuna, M.H., Ness, N.F., 1981. Modeling the Jovian current sheet and inner magnetosphere. J. Geophys. Res. 86, 8370–8384.
Cooper, J.F., Simpson, J.A., 1980. Sources of high-energy protons in Saturn's magnetosphere. J. Geophys. Res. 85, 5793–5802.
Fama, M., Loeffler, M.J., Raut, U., Baragiola, R.A., 2010. Radiation-induced amorphization of crystalline ice. Icarus 207, 314–319.
Hamilton, D.P., Burns, J.A., 1994. Origin of Saturn's E ring: self-sustained, naturally. Science 264, 550–553.
Hand, K.P., Carlson, R.W., 2011. H_2O_2 production by high energy electrons on icy satellites as a function of surface temperature and electron flux. Icarus 215, 226–233.
Hansen, G.B., McCord, T.B., 2004. Amorphous and crystalline ice on the Galilean satellites: a balance between thermal and radiolytic processes. J. Geophys. Res. 109, E01012.
Hendrix, A.R., Domingue, D.L., King, K., 2005. The icy Galilean satellites: ultraviolet phase curve analysis. Icarus 173, 29–49.
Hibbitts, C.A., McCord, T.B., Hansen, G.B., 2000. Distributions of CO_2 and SO_2 on the surface of Callisto. J. Geophys. Res. 105 22,541–22,557.
Howett, C.J.A., Spencer, J.R., Schenk, P., Johnson, R.E., Paranicas, C., Hurford, T.A., Verbiscer, A., Segura, M., 2011. A high-amplitude thermal inertia anomaly of probable magnetospheric origin on Saturn's moon Mimas. Icarus 216, 221–226.
Khurana, K.K., 1997. Euler potential models of Jupiter's magnetospheric field. J. Geophys. Res. 102, 11,295.
Khurana, K.K., Pappalardo, R.T., Murphy, N., Denk, T., 2007. The origin of Ganymede's polar caps. Icarus 191, 193–202.
Kollmann, P., Roussos, E., Paranicas, C., Krupp, N., Haggerty, D.K., 2013. Processes forming and sustaining Saturn's proton radiation belts. Icarus 222, 323–341.
Ligier, N., Poulet, F., Carter, J., Brunetto, R., Gourgeot, F., 2016. VLT/SINFONI observations of Europa: new insights into the surface composition. AJ 151, 163.
Mastrapa, R.M.E., Brown, R.H., 2006. Ion irradiation of crystalline $H_2$0-ice: effect on the 1.65μm band. Icarus 183, 207–214.
Mauk, B.H., Mitchell, D.G., McEntire, R.W., Paranicas, C.P., Roelof, E.C., Williams, D.J., Lagg, A., 2004. Energetic ion characteristics and neutral gas interactions in Jupiter's magnetosphere. J. Geophys. Res. 109 2003JA010270.
McCord, T.B., et al., 1998. Salts on Europa's surface detected by Galileo's near infrared mapping spectrometer. Science 280, 1242.
Moore, J.M., Mellon, M.T., Zent, A.P., 1996. Mass wasting and ground collapse in terrains of volatile-rich deposits as a solar system-wide geological process: the pre-Galileo view. Icarus 122, 63–78.
Moore, M.H., Hudson, R.L., 2000. IR detection of H_2O_2 at 80K in ion-irradiated laboratory ices relevant to Europa. Icarus 145, 282–288.
Moore, M.H., Hudson, R.L., 1992. Far-infrared spectral studies of phase changes in water ice induced by proton irradiation. Astrophys. J. 401, 353–360.
Newman, S.F., Buratti, B.J., Brown, R.H., Jaumann, R., Bauer, J., Momary, T., 2008. Photometric and spectral analysis of the distribution of crystalline and amorphous ices on Enceladus as seen by Cassini. Icarus 193, 397–406.
Pappalardo, R.T., et al., 2004. Geology of Ganymede. In: Bagenal, F., Dowling, T.E., McKinnon, W.B. (Eds.), Jupiter. Cambridge Univ Press, pp. 363–396.
Paranicas, C., et al., 2012. Energetic charged particle weathering of Saturn's inner satellites. Planet. Space Sci. 61, 60–65.
Roth, L., Saur, J., Retherford, K.D., Strobel, D.F., Feldman, P.D., McGrath, M.A., Nimmo, F., 2014. Transient water vapor at Europa's south pole. Science 343, 171–174.
Roussos, E., et al., 2008. Discovery of a transient radiation belt at Saturn. Geophys. Res. Lett. 35, L22106. doi:10.1029/2008GL035767.
Scipioni, F., Schenk, P., Tosi, F., D'Aversa, E., Clark, R., Combe, J.-PH., Dalle Ore, C.M., 2017. Deciphering sub-micron ice particles on Enceladus surface. Icarus 290, 183–200.
Seki, J., Hasegawa, H., 1983. The heterogeneous condensation of interstellar ice grains. Astrophys. Space Sci. 94, 177–189.
Sparks, W.B., Hand, K.P., McGrath, M.A., Bergeron, E., Cracraft, M., Deustua, S.E., 2016. Probing for evidence of plumes on Europa with HST/STIS. Astrophys. J. 829, 121.
Stephan, K., 2012. The Saturnian satellite Rhea as seen by Cassini VIMS. Planet. Space Sci. 61, 142–160.
Stephan, K., et al., 2010. Dione's spectral and geological properties. Icarus 206, 631–652.
Strazzulla, G., Baratta, G.A., Leto, G., Foti, G., 1992. Ion-beam-induced amorphization of crystalline water ice. Europhys. Lett. 18, 517.
Verbiscer, A., French, R., Showalter, M., Helfenstein, P., 2007. Enceladus: cosmic graffiti artist caught in the act. Science 315, 815.